

MODIS DATA STUDY TEAM PRESENTATION

September 22, 1989

AGENDA

1. Determination of Oceanic Primary Productivity
2. Determination of the Attenuation Coefficient of Photosynthetically Active/Available Radiation
3. Determination of Land Surface Temperatures
4. Earth Observing Scanner Polarimeter (EOSP) Instrument Performance Requirements
5. Update on the Error Analysis of MODIS Earth Navigation Issues

Determination of Oceanic Primary Production

Primary production is a measure of the rate of production of organic carbon in the oceans from CO₂, primarily by oceanic phytoplankton. It is important for two reasons. First, since phytoplankton form the base of the oceanic food web, their production determines the amount of food available for upper level organisms, including fish, shellfish, etc., and thus how much we can harvest from the sea. Second, since phytoplankton absorb CO₂, they act as a pathway of atmospheric CO₂ to the oceans. Thus they influence the global carbon budget and may affect the Earth's climate.

Despite its importance, primary production is extremely difficult to measure, especially on the large spatial scales important for global climate. It is the large areal coverage of satellite sensors, specifically MODIS, that make improved estimations of oceanic primary production feasible.

Methods for estimating primary production from remote sensing data may be grouped into two classes: empirical models relating production to remotely-sensed chlorophyll (an indicator of phytoplankton biomass), surface solar irradiance, sea surface temperature, etc. (e.g., Eppley et al., 1985; Balch et al., 1989), semi-analytical models using relationships involving these various environmental variables (e.g., Platt, 1986; Campbell and O'Reilly, 1987). However, the models have explained less than 50% of the variance in observations (Balch et al., 1989), suggesting that the estimation of primary production from space will be an intensive research program before, during, and even after the MODIS era.

Regarding empirical relationships, while several have been developed, many require in-situ data for calibration and fine-tuning. As such these are unacceptable for routine processing. Some, however, require only remotely-sensed variables, and in all cases listed below are derived strictly from remotely-sensed chlorophyll concentrations. In the following, P represents integrated water column production (mg carbon m⁻² day⁻¹) and C represents satellite-derived pigment concentrations (mg m⁻³).

Smith et al., 1982

$$P = 210C + 383 \quad (1)$$
$$r^2 = 0.32$$

Note: not applicable for $P < 383$ mg carbon m⁻² day⁻¹

Brown et al., 1985 (from Smith and Baker, 1977 and using Balch et al.'s (1989) computation for euphotic zone depth)

$$P = C^{0.73} [564.4 - 531.7 \log C] \quad (2)$$
$$r^2 = 0.28$$

Note: not applicable for $P > 690$ mg carbon m⁻² day⁻¹

Eppley et al., 1985

$$P = 1000C^{0.5} \quad (3)$$

(no r^2 reported)

Balch et al., 1989

$$P = 513C^{0.48} \quad (4)$$
$$r^2 = 0.35$$

The algorithms are intercompared in Figure 1 over a range of chlorophyll concentrations ordinarily encountered in the oceans. One may note a considerable difference in the estimated primary production from chlorophyll. Since only two of the algorithms, Eqns. 3 and 4, compute reasonable production estimates within the full range of chlorophyll values present in the ocean, these may be considered the best candidates for a core product algorithm at this time. Of these, Eqn. 3 produces much higher production estimates than Eqn. 4, especially at high chlorophyll ($> 1 \text{ mg m}^{-3}$).

Dr. Wayne Esaias hopes to use empirical equations such as those above to produce a core ocean data product for MODIS. However, he would like to refine the accuracy (increase the r^2) by including empirical relationships with sea surface temperature, surface incident photosynthetically available radiation (PAR), and the rate of attenuation of PAR in the water column (K_{PAR}), variables which are known to affect primary production and which should be available routinely from satellite observations (or derived therefrom). Such equations would have the form

$$\log P = a + \sum b_i \log x_i \quad (5)$$

where a is an empirically-determined intercept, b_i is the empirically-determined slope of the i th component, and x_i is the component (chlorophyll, SST, PAR, etc.). These relationships have yet to be determined.

It should be noted that all of the above relationships require that the satellite-observed chlorophyll (C), i.e., that in the first attenuation depth, is a constant fraction of total water column chlorophyll. Although this suggestion has been supported by some observations (Platt and Herman, 1983), deviations from it may explain the rather low coefficients of determination (r^2) in the relationships.

Regarding semi-analytic algorithms, while they are superior in principle to the empirical algorithms because they attempt to resolve causal processes affecting primary production, they have not as yet achieved a great deal of success in estimating primary production. Platt (1986) proposed a linear relationship between integrated water column production and surface light intensity (PAR). The relationship assumed that chlorophyll concentrations were uniform with depth, and that depth-integrated chlorophyll

biomass could be determined from surface (or satellite-detected) chlorophyll. From Platt (1986)

$$P = \phi S \quad (6)$$

and

$$S = \text{PAR}(k_c C_T / K_{\text{PAR}}) \quad (7)$$

where ϕ is the quantum yield of light absorption (moles of carbon produced per mole photons absorbed), k_c is the specific absorption coefficient of chlorophyll (normalized to unit biomass), C_T is depth-integrated chlorophyll, and other variables are as defined above. ϕ is estimated a priori given knowledge of the maximum quantum yield and is assumed constant, k_c is estimated a priori from the literature, and the other independent variables are obtainable from the satellite, assuming depth-independent chlorophyll distributions. Conforming to the assumption of linearity between production and PAR, Platt defines $\psi = P/(C_T \text{ PAR})$, which he suggested should be constant. However, Campbell and O'Reilly (1988) found that ψ varied substantially and also that ϕ was not a constant fraction of the maximum quantum yield. Thus such semi-analytical algorithms are subject to substantial errors and require further research, which Dr. Abbott proposes.

Dr. Mark Abbott proposes to develop new relationships between fluorescence and primary production in conjunction with other models. The principle is that chlorophyll fluoresces when the photosystems of phytoplankton are saturated, i.e., when no more photons may be used for production. Thus the amount of fluorescence should be inversely related to primary production. These relationships have not yet been developed.

References

- Balch, W.M., M.R. Abbott, and R.W. Eppley, 1989. Remote sensing of primary production--I. A comparison of empirical and semi-analytical algorithms. *Deep-Sea Research* 36: 281-295.
- Brown, O.B., R.H. Evans, J.W. Brown, H.R. Gordon, R.C. Smith, and K.S. Baker, 1985. Phytoplankton blooming off the U.S. East Coast: a satellite description. *Science* 229: 163-167.
- Campbell, J.W. and J.E. O'Reilly, 1988. Role of satellites in estimating primary productivity on the northwest Atlantic continental shelf. *Continental Shelf Research* 8: 179-204.
- Eppley, R.W., E. Stewart, M.R. Abbott, and U. Heymann, 1985. Estimating ocean primary production from satellite chlorophyll. Introduction to regional differences and statistics for the Southern California Bight. *Journal of Plankton Research* 7: 57-70.
- Platt, T., 1986. Primary production of the ocean water column as a function of surface light intensity: algorithms for remote sensing. *Deep-Sea Research* 33: 149-163.

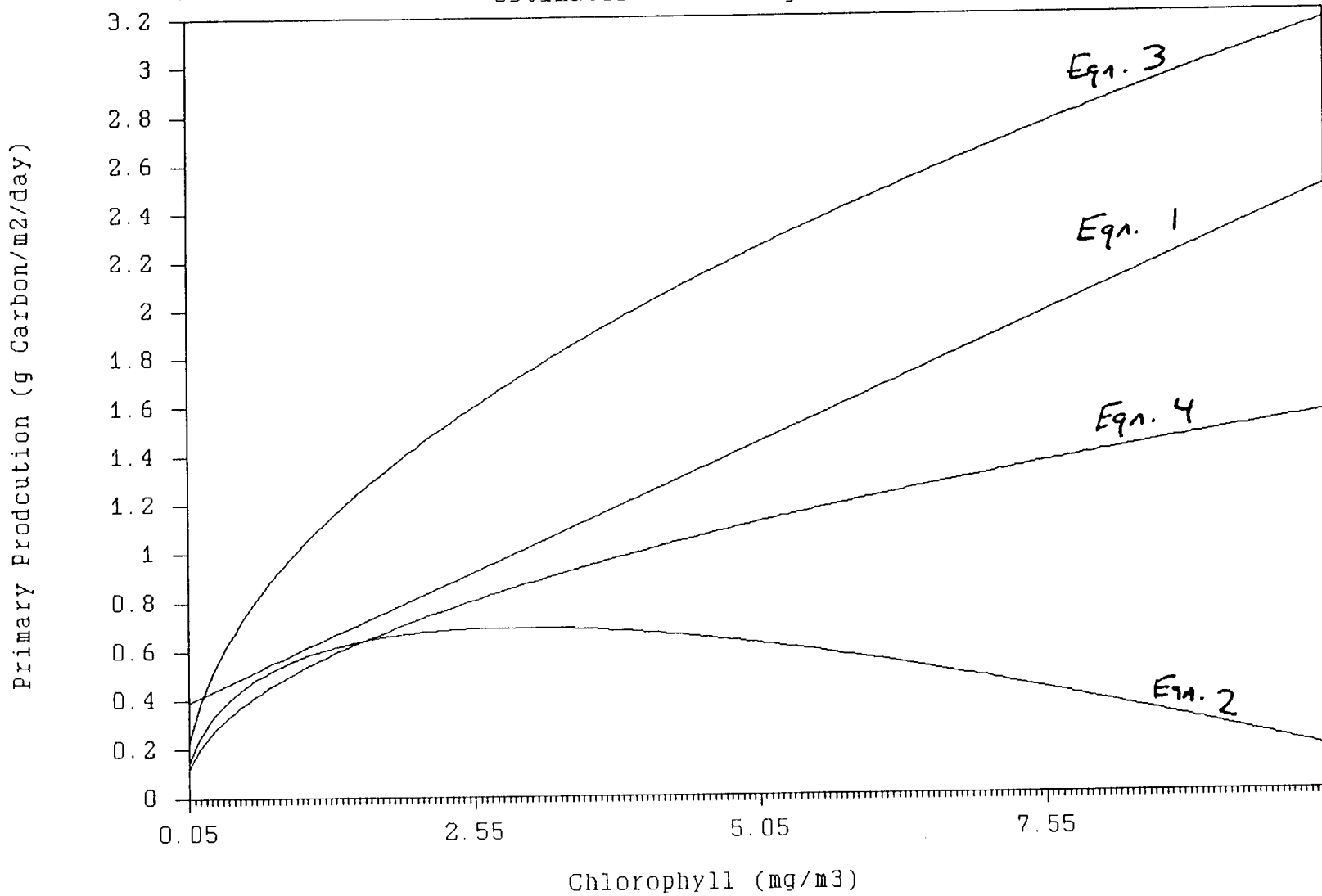
Platt, T. and A.W. Herman, 1983. Remote sensing of phytoplankton in the sea: surface-layer chlorophyll as an estimate of water-column chlorophyll and primary production. *International Journal of Remote Sensing* 4: 343-351.

Smith, R.C., and K.S. Baker, 1977. The bio-optical state of ocean waters and remote sensing. Scripps Institution of Oceanography Technical Report No. 77-2, San Diego, Cal. 35 pp.

Smith, R.C., R.W. Eppley, and K.S. Baker, 1982. Correlation of primary production as measured aboard ship in Southern California coastal waters and as estimated from satellite chlorophyll images. *Marine Biology* 66: 281-288.

Figure 1. Primary production

estimates from 4 algorithms.



Determination of the Attenuation Coefficient of
Photosynthetically Available Radiation (K_{PAR})

K_{PAR} , the attenuation coefficient of downwelling photosynthetically available radiation (PAR; the flux of quanta, or photons, from 400 to 700 nm) is a measure of the rate at which quanta are removed from the water column. It is formally defined as

$$K_{PAR} = 1/PAR \, d(PAR)/dz \quad (1)$$

and PAR is formally defined as

$$PAR = 1/hc_s \int_{400}^{700} \lambda E_d(\lambda) \, d\lambda, \quad (2)$$

where h is Planck's constant, c_s is the speed of light, and $E_d(\lambda)$ is the downwelling irradiance expressed as the flux of energy. Since phytoplankton absorb quanta, K_{PAR} is critical for determining the amount of quanta at depth in the water column, and hence the amount of photosynthesis, or growth of phytoplankton, that is possible. The growth of phytoplankton, in turn, is responsible for oceanic primary production.

There is only one method proposed for determining K_{PAR} for MODIS. Dennis Clark proposes to determine it directly from in-situ measurements of downwelling irradiance from a system of optical buoys. These data will be made available through EosDIS. Although this will provide a reliable set of data, a system of buoys will not produce the areal coverage required for the estimation of large scale primary production.

No specific algorithm has been developed or proposed for deriving K_{PAR} from remote sensing platforms. However, by inverting relationships between normalized water-leaving radiances and chlorophyll concentrations, given by Gordon et al. (1988), one may derive a possible method for determining K_{PAR} from remotely sensed water-leaving radiance. The relationship requires a substantial number of independent variables, but all are either known a priori or are derivable directly from the water-leaving radiance output from MODIS. The relationship applies only to Case 1 waters, where the optical properties are dominated by chlorophyll and associated detrital material.

A full derivation of the method is attached, but the final result is presented here. K_{PAR} may be considered the mean of $K(\lambda)$ over the wavelength range 400 to 700 (Sathyendranath and Platt, 1988), and $K(\lambda)$ is determinable from relationships given in Gordon et al. (1988). The relationship is

$$K(\lambda) = 0.110 \, b_b(\lambda) \, F_o(\lambda) \, (1-\rho)(1-\rho_o) \, (n^2 [L_w(\lambda)]_N)^{-1} \quad (3)$$

where $b_b(\lambda)$ is the backscattering coefficient, $F_o(\lambda)$ is the instantaneous extraterrestrial irradiance, ρ is the Fresnel

reflectance of the sea surface for normal incidence, ρ_o is the Fresnel reflectance of the sea surface for direct and diffuse solar irradiance, n is the refractive index for seawater, and $[L_w(\lambda)]_N$ is the normalized water-leaving radiance. $[L_w(\lambda)]_N$ is related to the water-leaving radiance detected at the sensor by

$$[L_w(\lambda)]_N = L_w(\lambda)/t(\lambda, \theta_o) \cos \theta_o \quad (4)$$

where $t(\lambda, \theta_o)$ is the diffuse transmittance of the atmosphere (ignoring aerosols), defined by

$$t(\lambda, \theta_o) = \exp[-(\tau_r(\lambda)/2 + \tau_{Oz}(\lambda))]/\cos \theta_o \quad (5)$$

and τ_r is the Rayleigh scattering optical thickness and τ_{Oz} the ozone optical thickness; both are available through the atmospheric correction algorithm. θ_o in Eqns. 3 and 4 is the solar zenith angle.

The backscattering coefficient is the key to solving Eqn. 3. It is the sum of the backscattering coefficients of all the optical constituents in the water, which, for Case 1 waters, are only water and chlorophyll (and their associated detrital pigments)

$$b_b(\lambda) = [b_b(\lambda)]_w + [b_b(\lambda)]_p \quad (6)$$

where $[b_b(\lambda)]_w$ is the backscattering from water and $[b_b(\lambda)]_p$ is the backscattering due to chlorophyll-containing particles. $[b_b(\lambda)]_w$ is known a priori from Morel (1974). Gordon et al. (1988) determine the backscattering coefficient for particles $[b_b(\lambda)]_p$ from

$$[b_b(\lambda)]_p = A(\lambda) C^{B(\lambda)} \quad (7)$$

where A and B are constants relating backscattering efficiency to chlorophyll concentration (C), determined a priori.

All of the terms in Eqn. 3 are now either known a priori or determined by the satellite. Eqn. 3 is thus a closed system whereby $K(\lambda)$, and then K_{PAR} can be obtained.

For processing, a set of $A(\lambda)$'s and $B(\lambda)$'s will have to be generated for the wavelength bands of MODIS. ρ , ρ_o , and n may be taken as constants.

Derivation

Gordon (1986) found through a series of computations that the downwelling attenuation coefficient $K(\lambda)$ may be expressed by

$$K(\lambda) = 1.054 D_0 (a(\lambda) + b_b(\lambda)) \quad (8)$$

to within about 1%. In Eqn. 8, D_0 is the downwelling irradiance distribution function, $a(\lambda)$ is the absorption coefficient of water plus chlorophyll and associated pigments, and $b_b(\lambda)$ is the backscattering coefficient. Gordon et al. (1988) also found that the irradiance reflectance, R ($= E_w/E_d$, the ratio of upwelling irradiance to downwelling irradiance just below the sea surface) may be expressed as

$$R = 0.0949 Q b_b(\lambda) / (a(\lambda) + b_b(\lambda)) \quad (9)$$

with a maximum error of about 16% for solar zenith angles $\geq 20^\circ$. In Eqn. 9, Q is the ratio of the upwelling irradiance to the upwelling radiance, and equals π for a perfectly diffuse light field.

Combining Eqns. 8 and 9, we find that

$$K = 0.1 D_0 Q b_b 1/R \quad (10)$$

where λ -dependences are now suppressed. D_0 ranges between 1.0 and 1.2 for small solar zenith angles. If we let $D_0 = 1.1$, Eqn. 10 reduces to

$$K = 0.11 Q b_b 1/R \quad (11)$$

Now, R may be expressed in terms of the normalized water-leaving radiance (water-leaving radiance detected at the satellite with the atmosphere removed and at a nadir solar zenith angle) by

$$R = n^2 Q [L_w(\lambda)]_N \{(1-\rho)(1-\rho_o) F_o(\lambda)\}^{-1} \quad (12)$$

if one ignores reflection of upwelling light by the sea surface, which is considered unimportant (Gordon et al., 1988). By adding the atmosphere and using the correct solar zenith angle, one may obtain a similar expression for the remotely-sensed water-leaving radiance. Substituting Eqn. 12 into Eqn. 11, we obtain an expression for K in terms of the normalized water-leaving radiance, a variable determined by satellite observation:

$$K(\lambda) = 0.11 b_b(\lambda) F_o(\lambda) (1-\rho)(1-\rho_o) \{n^2 [L_w(\lambda)]_N\}^{-1} \quad (13)$$

re-inserting the λ -dependence. Taking the mean of $K(\lambda)$ over all measured spectral bands within the range 400-700 nm, one may obtain K_{PAR} .

References:

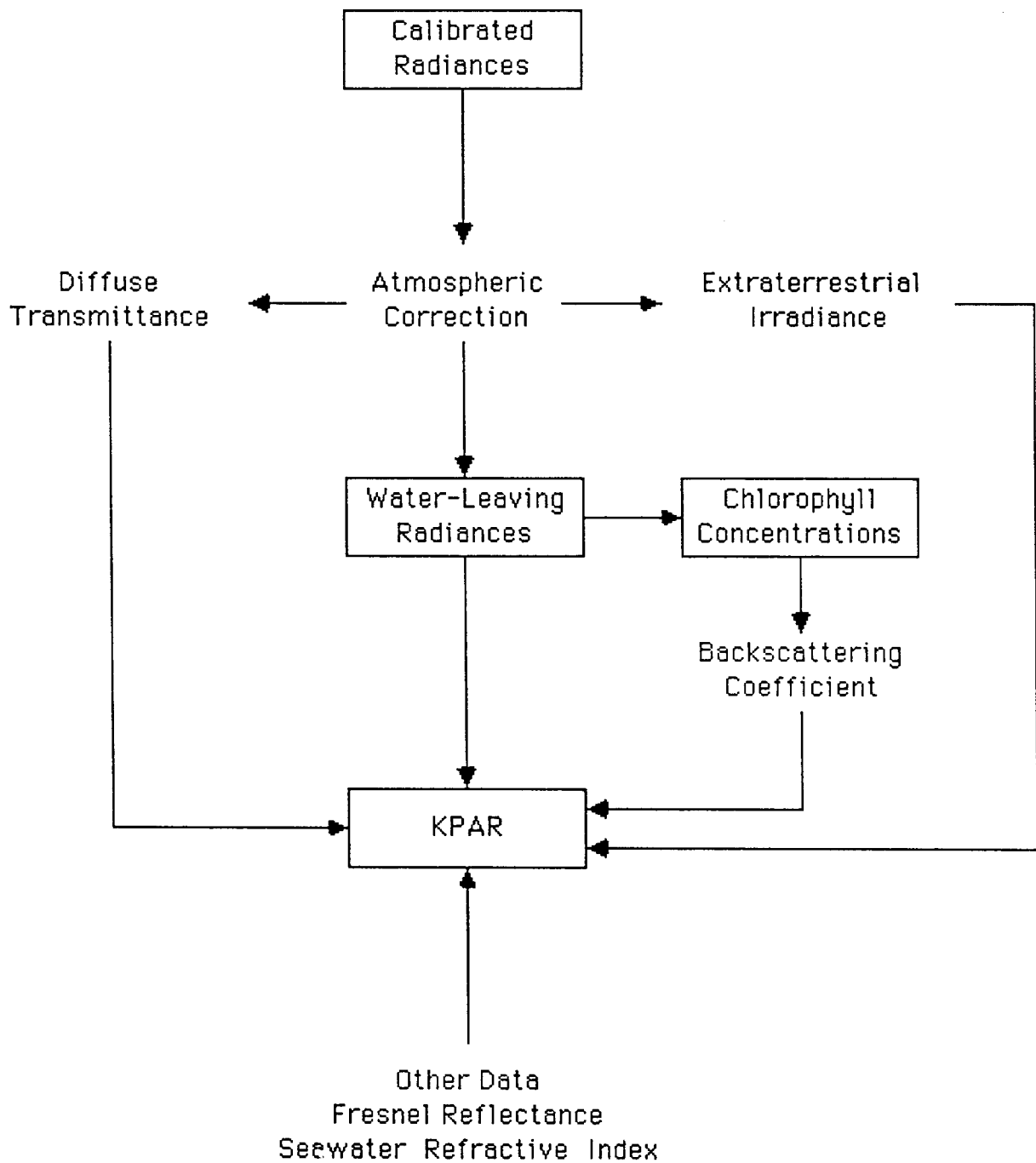
Gordon, H.R., 1986. Ocean color remote sensing: influence of the particle phase function and the solar zenith angle. EOS, Transactions of the American Geophysical Union 14: 1055.

Gordon, H.R., O.B. Brown, R.H. Evans, J.W. Brown, R.C. Smith, K.S. Baker, and D.K. Clark, 1988. A semianalytic radiance model of ocean color. Journal of Geophysical Research 93: 10909-10924.

Morel, A., 1974. Optical properties of pure water and pure seawater. In: Optical aspects of oceanography, N.G. Jerlov and E. Steeman-Nielsen, eds. Academic Press, San Diego, Cal., pp 1-24.

Sathyendranath, S. and T. Platt, 1988. The spectral irradiance field at the surface and in the interior of the ocean: a model for applications in oceanography and remote sensing. Journal of Geophysical Research 93: 9270-9280.

Determination of KPAR



DETERMINATION OF LAND SURFACE TEMPERATURE

In contrast to the Sea Surface Temperature (SST) problem, which has been much researched and involves a surface medium of (relatively) known properties, the estimation of land surface temperatures is a much more difficult problem because of effects related to atmospheric attenuation, surface emissivity, and topography. Since land surface temperatures of the desired accuracy have not yet been achieved in a working algorithm, the information that follows is tentative and subject to revision.

Assuming that surface emissivities are known to first order, the following equation can be derived relating the blackbody surface radiance in a hypothetical instrument with six thermal bands to observed radiance values in bands 1, 4, and 6

$$\begin{aligned}
 L_{s,4}(4, 1, 6) = & (0.1048L_1 - 0.098L_6) \mu^{-1} + \left(\frac{L_1}{\epsilon_1} - \frac{L_4}{\epsilon_4} \right) \\
 & \times \left\{ \left[0.0243 \left(\frac{L_6}{\epsilon_6} - \frac{L_4}{\epsilon_4} \right) + 0.0237 \right] \right. \\
 & \cdot \left. \mu^{-1} - \frac{0.4226}{L_1} + 0.3513 \right\} - \left(\frac{L_6}{\epsilon_6} - \frac{L_4}{\epsilon_4} \right) \\
 & \cdot \left[0.3031 \left(\frac{L_6}{\epsilon_6} - \frac{L_4}{\epsilon_4} \right) + \frac{7.0186}{L_6} \right. \\
 & \left. - 0.1509 \right] + \left(\frac{0.2255}{\epsilon_6} - 0.229 \right) L_6 \\
 & + 0.2859L_4 + 0.7411L_1 - 0.096
 \end{aligned}$$

where $L_{s,4}$ is the blackbody radiance in band 4, corrected for atmosphere and emissivity. (Similar equations can be derived for other bands). The corrected radiance (and assumed emissivity) can then be used to solve for the surface temperature T_s by inverting the Planck equation:

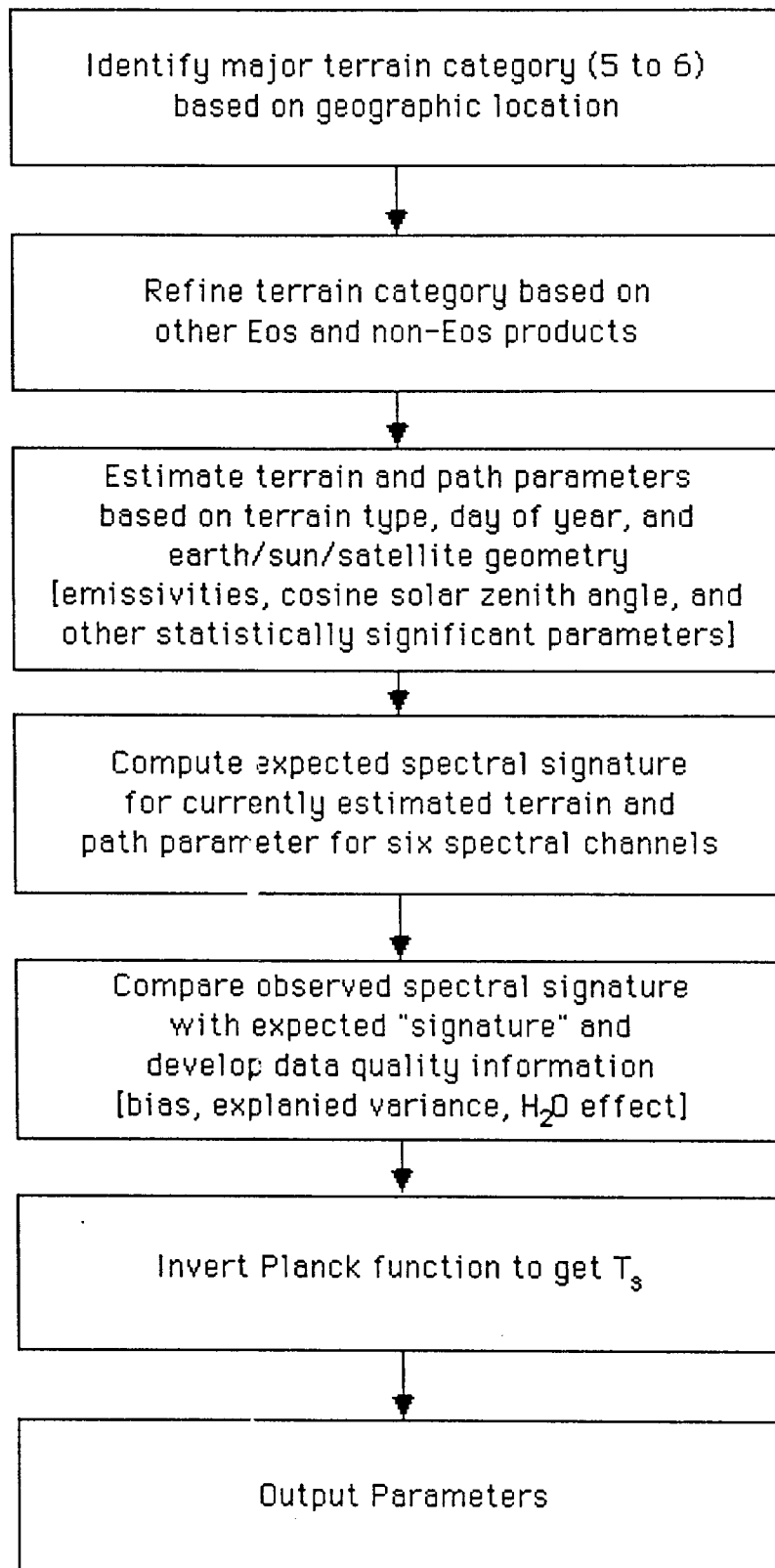
$$L(\lambda, T) = \epsilon(\lambda)B(\lambda, T_s) = \epsilon(\lambda) \frac{2hc^2}{\lambda^5 (e^{hc/\lambda kT_s} - 1)}$$

Temperatures obtained in this manner are sensitive to errors in assumed emissivity (the temperature error associated with a 0.01 uncertainty in emissivity is larger than the error in the atmospheric correction model). Assuming that thermal data are combined with other with other remotely sensed data to classify terrain as either clay, fine sands, coarse sands, tree leaf, or snow, and assuming that clay and sands have spectral emissivity features and that tree leaves and snow are spectrally flat, complicated equations containing more than 30 terms and involving four thermal bands, but not explicitly containing emissivity, are obtained. For these conditions, surface temperatures are estimated to a maximum error or less than 1 degree K.

REFERENCES:

1. Wan, Zhengming, and Jeff Dozier, Land-Surface Temperature Measurement from Space: Physical Principles and Inverse Modeling, IEEE Transactions on Geoscience and Remote Sensing, Vol. 27, No. 3, May 1989
2. Wan, Zhengming, Land Surface Temperature Measurements from Eos MODIS Data, Proposal submitted to the National Aeronautics and Space Administration, June 15, 1988

Major Structure of Land-Surface Temperature Algorithm



EARTH OBSERVING SCANNING POLARIMETER (EOSP)
INSTRUMENT PERFORMANCE REQUIREMENTS
MAY 24, 1989

1.0 Introduction

The Earth Observing System (Eos) is an international program which will develop and deploy observing platforms in order to obtain a comprehensive data base of remote sensing measurements from space on a global scale for a period of at least ten years. Eos will also develop the large-scale data and information system necessary to facilitate the integrated multidisciplinary studies of the entire Earth system. The first Eos operational platform is the NASA polar orbiting platform, NPOP-1, currently scheduled for launch in December, 1996. NPOP-1 will carry a complement of facility instruments and selected Principal Investigator instruments, with the specific payload to be confirmed after definition studies. The Earth Observing Scanning Polarimeter (EOSP) is one of the PI instruments selected for possible flight on NPOP-1. EOSP is a high-precision, multi-channel, scanning photopolarimeter designed to address key Eos science objectives by measuring the radiance and linear polarization of reflected sunlight.

2.0 Objectives

The objective of the EOSP experiment is to obtain global maps of the radiance and linear polarization for twelve spectral bands in the visible and near infrared in order to:

- (1) determine cloud properties including optical thickness, particle size, liquid/ice phase, and cloudtop pressure;
- (2) determine the global distribution and optical thickness of the tropospheric and stratospheric aerosols;
- (3) provide atmospheric correction information for ocean and land observations; and
- (4) investigate the potential for providing information on vegetation and land characteristics.

One of the key science tasks for the Eos mission is to characterize the large-scale and low-frequency variability of clouds and to determine the effect of clouds on the net incoming solar radiation and the net outgoing long-wave radiation. Information inherent in global maps of radiance and linear polarization of reflected sunlight will permit the compilation of a systematic climatology of critical cloud parameters essential for quantifying the radiative role of clouds. Analyses of the EOSP observations will allow the routine determination of cloud optical thickness, particle size and phase at the top of the cloud, and the pressure level of the cloudtop.

The characterization of the global distribution of aerosols is another of the important Eos science objectives. EOSP polarization measurements will constitute a very sensitive detector of the presence of aerosols. One of the EOSP objectives will be the determination of the global distribution and optical thickness of the stratospheric aerosols and the same information for tropospheric aerosols for cloud-free conditions. A valuable by-product of the

characterization of the aerosols is the potential for improved atmospheric corrections. Virtually all satellite remote sensing of land and oceans at visible and near-infrared wavelengths requires a correction to remove effects of molecular and aerosol scattering. Although various empirical approaches, typically involving ratioing of normalized radiances in different spectral bands, have been employed for making atmospheric correction estimates, the optimum approach is based on corrections computed using radiative transfer models which include detailed specification of the aerosol optical properties.

3.0 Instrument Requirements

3.1 Key Features

To accomplish the scientific objectives of the EOSP experiment we require a polarimeter that has the following key features:

- (1) simultaneous detection of orthogonal linear polarization components of the scene radiance;
- (2) capability to interchange the roles of corresponding detector elements used to detect orthogonal polarization components;
- (3) spatial coverage from limb to limb to provide global polarization maps;
- (4) simultaneous measurement in all 12 spectral bands;
- (5) simultaneous measurement of both the 0°/90° and 45°/135° linear polarization components;
- (6) instrumental polarization that is both small and varies only slightly with scan angle with a method to measure the instrumental polarization in flight as well as pre-flight;
- (7) single instantaneous field of view for the above measurements to assure automatic spatial registration of the polarimetric data; and
- (8) inflight calibration sources and methods adequate to provide radiometric calibration and polarimetric calibration.

3.2 Spectral Coverage

The EOSP shall make simultaneous measurements of radiance and linear polarization in 12 solar reflectance channels in the spectral range, 400 to 2300 nanometers as indicated below:

Channel	Wavelength (nm)	Bandwidth (FWHM, nm)
1	410	30
2	470	20
3	555	20
4	615	15
5	675	20
6	750	15
7	880	20
8	950	20
9	1250	60
10	1600	60
11	2050	100
12	2250	100

Channels 1 - 8 are designated as visible and near-infrared (VINIR) bands and channels 9 - 12 as shortwave infrared (SWIR) bands. The characteristics of the spectral bands shall be fully defined including in-band and out-of-band transmission, passband shape, and slopes of the band edges.

3.3 Field of View

The EOSP shall have an instantaneous field of view (IFOV) defined by a circular aperture of 14.2 mrad, yielding a 10-km nadir footprint for a 705-km orbital altitude. The IFOV shall be scanned from limb to limb in a direction perpendicular to the groundtrack of the NPOP-1 platform, with consecutive scans acquired approximately every 1.5 seconds. Simultaneous scene sampling for all 12 spectral channels shall be performed approximately every 3 ms during the limb to limb scan. Boresight alignment of the IFOVs for the 12 EOSP spectral channels shall differ by no more than 0.5 mrad.

3.4 Dynamic Range and Quantization

The dynamic range of the EOSP instrument shall be broad enough to cover scene reflectance variation corresponding to albedo ranging from 0.05 to 1.0 for all EOSP spectral channels. Detector outputs constituting the scene samples shall be digitized with 14-bit A/D conversion. A minimum of three commandable gain settings with relative gain factors of two and four, respectively, shall be provided. The root mean square signal to noise in each spectral channel when the EOSP views a scene of albedo 0.3 shall equal or exceed 2000.

3.5 Radiometric Accuracy

Digitized and calibrated EOSP radiances corresponding to typical scene samples shall have an absolute radiometric accuracy of 5% or better, with a design goal of 3% or better. It is presumed that this requirement will be met using pre-flight radiometric calibration with a traceable standard source and with on-board calibration using internal lamps and a solar diffuser source.

3.6 Polarimetric Accuracy

The four digitized detector outputs corresponding to a single scene measurement for a given EOSP spectral channel shall permit the calculation of the linear polarization with an accuracy of 0.2% or better for scenes of linear polarizance between 0 and 15%, with a design goal of 0.1%. Instrumental polarization must be determined and monitored with sufficient accuracy to maintain this required polarimetric accuracy. It is presumed that this requirement will be met using pre-flight calibration with ground support equipment constructed to provide a precisely known linear polarization and with viewing of on-board calibration sources.

3.7 On-Board Calibration

The EOSP instrument design shall incorporate three small tungsten filament lamps located in the scanning mirror housing and viewed in the portion of the scan during which the Earth is not viewed. It shall be a design objective contingent on instrument-platform interface considerations to provide as part of the EOSP system, a solar diffuser structure which can move a diffuse reflecting surface into the scanned swath. The solar diffuser target would be

so deployed and viewed as an inflight calibration source when illuminated by the sun during the polar pass portion of the NPOP-1 platform orbit.

3.8 Scattered Light

The EOSP shall be designed to provide rejection of off-axis illumination of the instrument detectors due to scattered or diffracted light. When the EOSP views a relatively uniform scene with an albedo of approximately 0.3, the fraction of the signal originating from beyond 5 mrad from the edge of the IFOV shall be less than 1% of that from within the IFOV.

3.9 Command and Control Functions

The EOSP electronics system design shall provide for receipt of ground commands to program an integral on-board processor to perform the following functions as a minimum: (1) standby mode select (scan motor off); (2) gain selection; (3) solar diffuser measurement cycle; (4) polarimetric calibration cycle; (5) calibration lamp #1, #2, and #3 ON/OFF; (6) radiative cooler Earth shield and cover latch release; and (7) solar diffuser latch release.

4.0 Preliminary EOSP Conceptual Design

The proposed EOSP instrument is based upon a preliminary conceptual design that is intended to meet the requirements imposed by the science objectives, but at the same time emphasizing the simplification of the design where possible and the use of proven techniques and existing space-qualified hardware. It is expected that the refinement of the conceptual design shall continue to use this emphasis in order to minimize development risk and cost and to enhance the overall system reliability.

The EOSP scanning system provides a continuous cross-track scan motion that allows limb-to-limb viewing and dc-restoration plus calibration source viewing during the backscan portion of the 360° rotation. The twin scan mirror assembly design provides polarization compensation at all scan angles. Eight bore-sighted telescope/aft optics assemblies provide the required spatial, spectral and polarization separations of the scanned scene. Each assembly contains a baffle system, refractive telescope, field stop, relay lens, and Wollaston prism to define the field of view and separate the incident scene flux into two orthogonally-polarized, angularly-separated beams. These beams are spectrally separated into three spectral bands using two dichroic beamsplitters and three bandpass filters. Each pair of polarized and spectrally defined beams are focused on either a dual-detector, silicon photodiode detector package (for the eight VNIR spectral bands) or a pair of HgCdTe photodiode detectors located on the cold (200 K) focal plane (for the four SWIR spectral bands).

The telescope/aft optics assemblies are grouped in pairs with each pair covering three spectral bands, with the octagonal telescope mount providing the proper orientation to allow simultaneous polarization sampling of the 0°/90° and 45°/135° polarization azimuths. Four achromatic half-wave retarders located on a retarder wheel provide occasional cross-calibration of the detectors used to measure the orthogonal polarization components. This occurs when the wheel position is rotated by 45° during a commanded calibration cycle.

A simple, single-stage radiation cooler provides the required focal plane cooling for the HgCdTe detectors and associated preamplifiers. The radiation cooler earth shield in its launch configuration will serve as a contamination cover. With the exception of the preamplifiers located with the optics, the remaining electronics (providing the signal processing and formatting, command and control, actuator driver circuitry, and power conditioning) are located in the electronics module portion of the instrument. The solar diffuser will be mounted on a light-weight frame attached to the optics housing. Upon command the solar diffuser can be driven from its protected configuration into the scanned swath for solar calibration near the south pole.

Update on the Error Analysis of MODIS Earth Navigation Issues

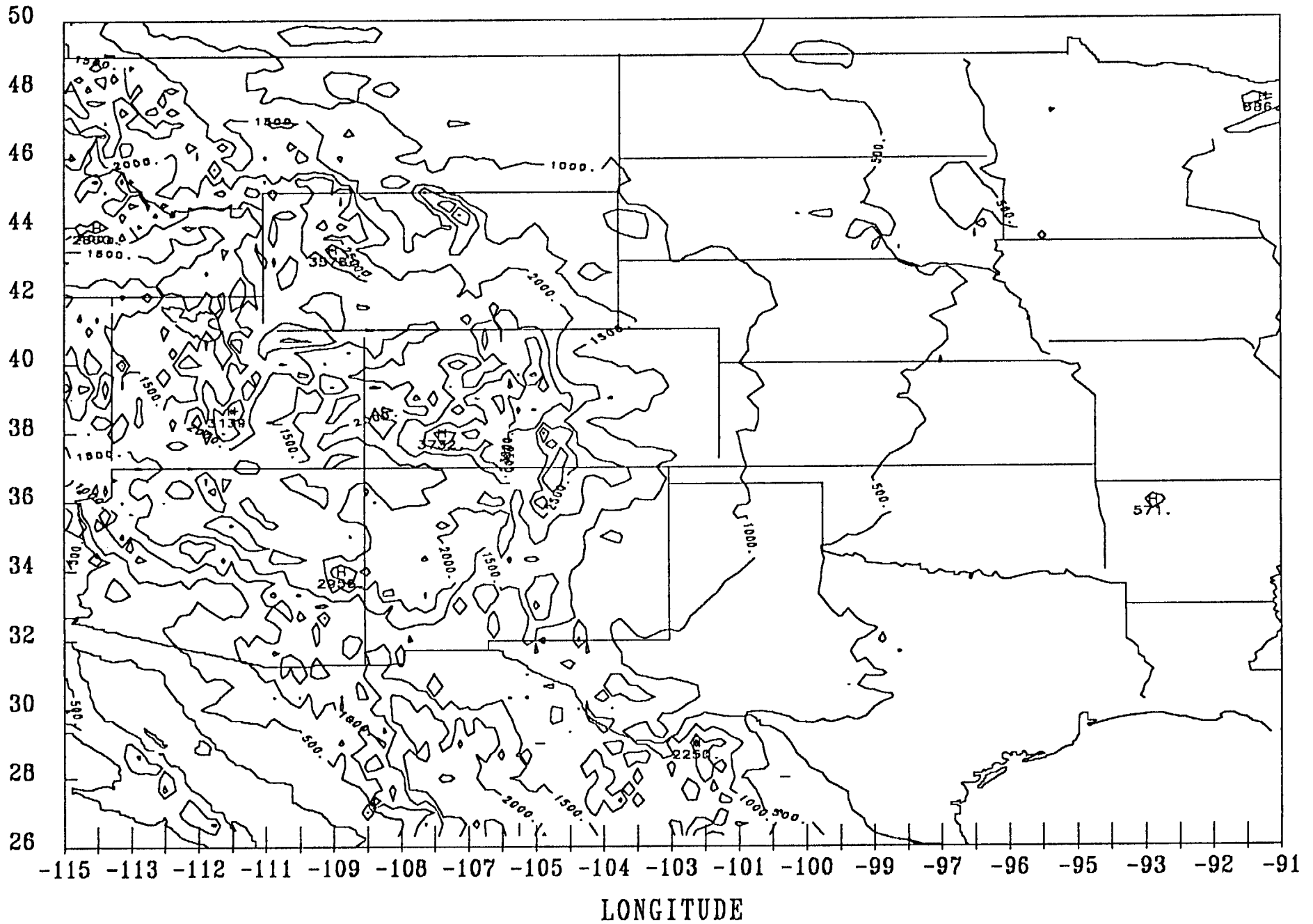
Having previously reported on the global 5-minute digital elevation data set, displaying representative regions (e.g, the eastern US at an earlier meeting, and demonstrating the capability to Earth locate MODIS IFOV centers, we now combine these capabilities.

Two regions are considered for demonstration purposes: the central US, including the Great Plains, and the western US, including the Rocky mountains. Two effects due to non-ellipsoidal topography occur: (1) horizontal pixel displacements and (2) illumination and other reflectance changes due to the surface slope. Here, we consider representative horizontal pixel displacements.

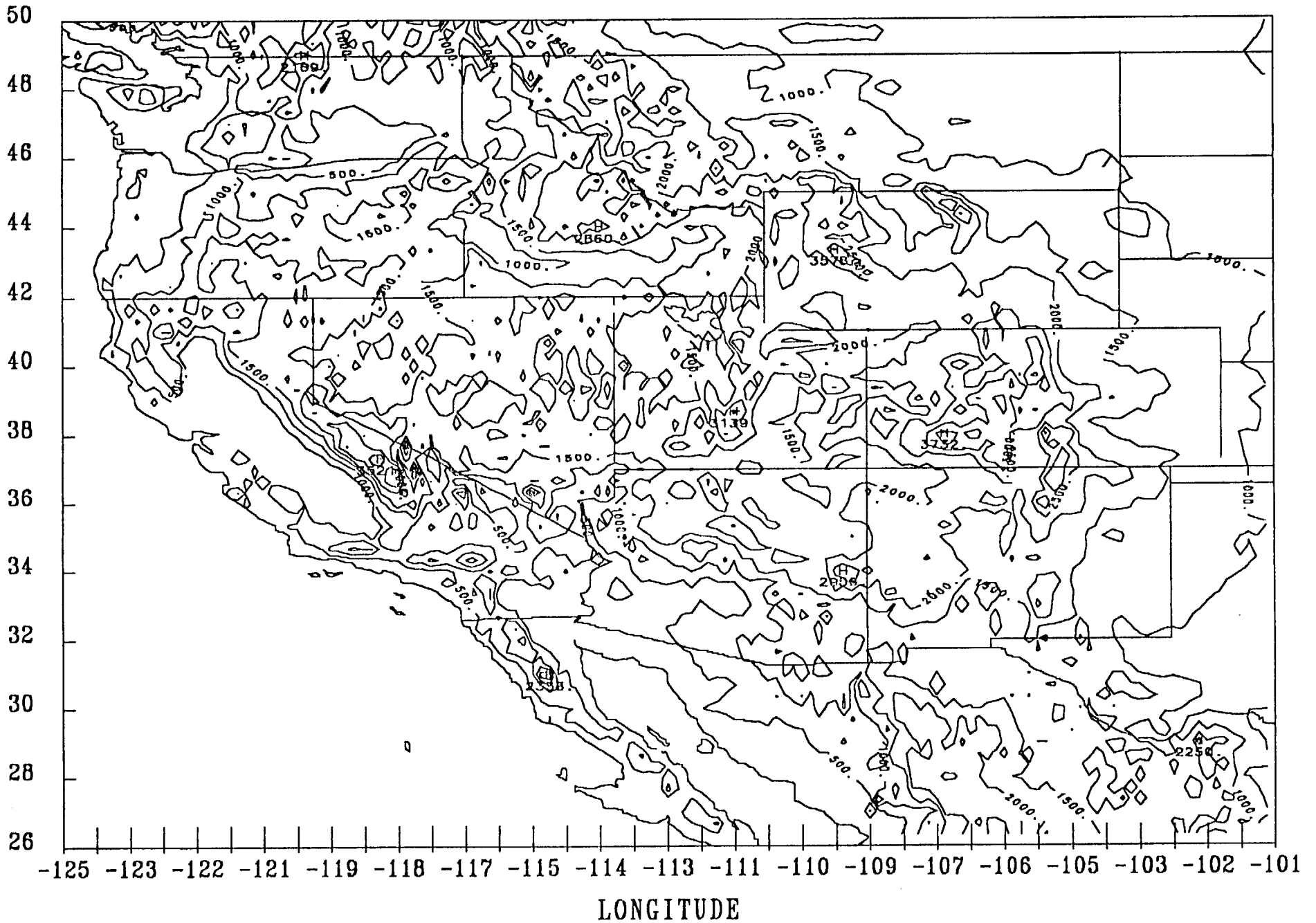
Figures 1 and 2 illustrate the surface topography (m) for the Central and Western US, respectively. The Great Plains region is characterized, at this resolution, by a shallow east-west gradient in elevation from less than 500 m to 1500 m over 10° to 15° of longitude. In contrast, the western US is characterized by elevations reaching 3000 m to 4000 m, except near coastal California.

Figures 3 and 4 show the apparent horizontal cross-track IFOV mislocations (m) that result with the specified topography for the two sub-satellite tracks shown. In Figure 3, with a satellite longitude of around 104° W, "relatively small errors are encountered near nadir (<500 m). Errors larger than 500 m occur to the east due to the high zenith angles, even for relatively low-lying areas. Errors exceeding 2,000 to 3,000 m occur to the west of the track. In Figure 4, for an orbit near 114° W, errors over the Rocky mountains are reduced due to the more-vertical views. However, once again, errors exceeding 2,000 to 3,000 m are encountered off nadir, and reach 4,400 m over Colorado near Pike's Peak.

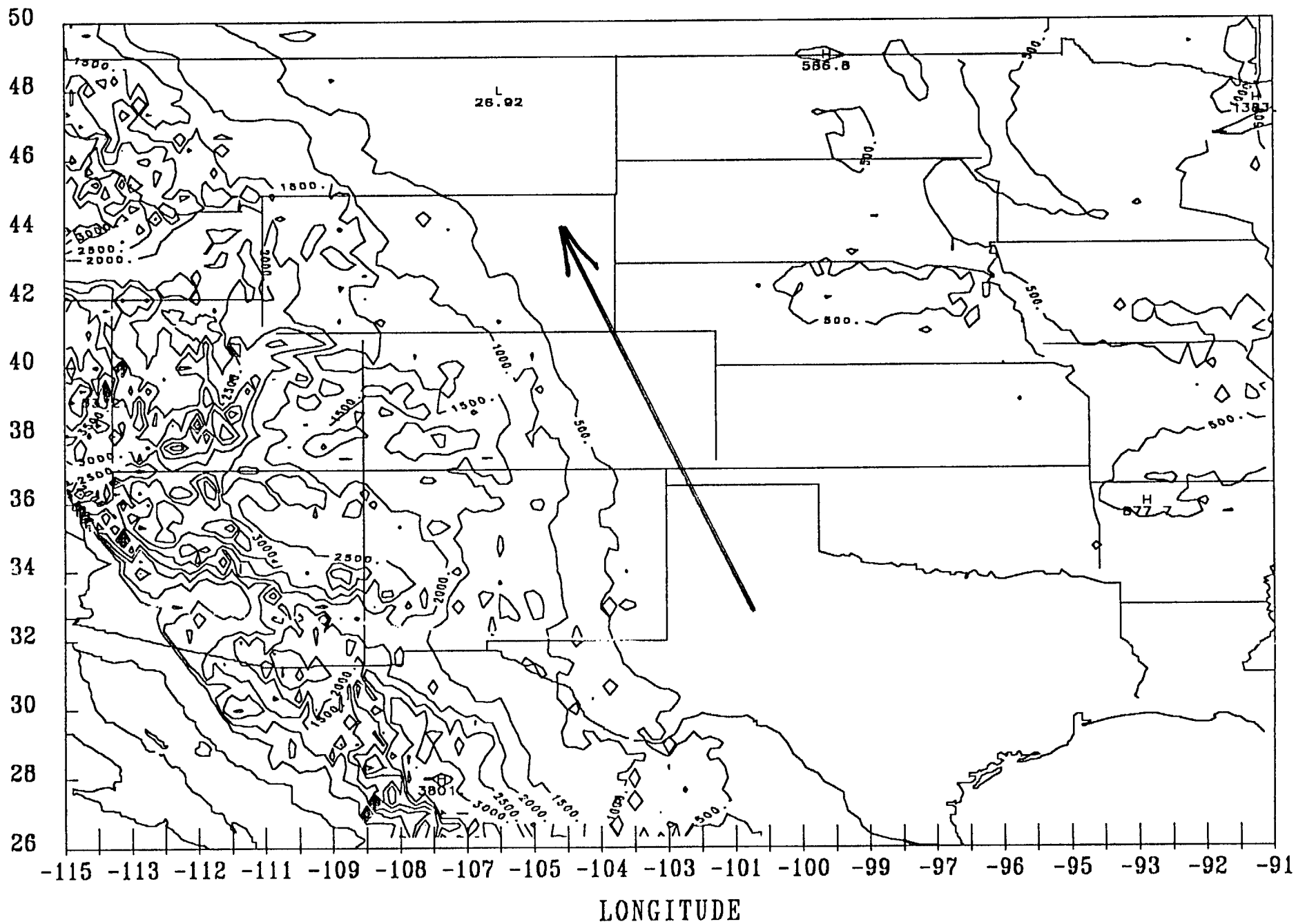
WORLD TOPOGRAPHY



WORLD TOPOGRAPHY



WORLD TOPOGRAPHY



WORLD TOPOGRAPHY

